

DMAT: An End-to-End Framework for Joint Atmospheric Turbulence Mitigation and Object Detection

Paul Hill, Alin Achim, Dave Bull, and Nantheera Anantrasirichai
Visual Information Laboratory, University of Bristol, Bristol, UK

Abstract

Atmospheric Turbulence (AT) degrades the clarity and accuracy of surveillance imagery, posing challenges not only for visualization quality but also for object classification and scene tracking. Deep learning-based methods have been proposed to improve visual quality, but spatio-temporal distortions remain a significant issue. Although deep learning-based object detection performs well under normal conditions, it struggles to operate effectively on sequences distorted by atmospheric turbulence. In this paper, we propose a novel framework that learns to compensate for distorted features while simultaneously improving visualization and object detection. This end-to-end framework leverages and exchanges knowledge of low-level distorted features in the AT mitigator with semantic features extracted in the object detector. Specifically, in the AT mitigator a 3D Mamba-based structure is used to handle the spatio-temporal displacements and blurring caused by turbulence. Features are extracted in a pyramid manner during the mitigation stage and passed to the detector. Optimization is achieved through back-propagation in both the AT mitigator and object detector. Our proposed DMAT outperforms state-of-the-art AT mitigation and object detection systems up to a 15% improvement on datasets corrupted by generated turbulence.

1. Introduction

When the temperature difference between the ground and the air increases, the thickness of each air layer diminishes, and they ascend rapidly. This leads to rapid micro-scale changes in the air's refractive index that degrade the visual quality of video signals and in turn impacting the effectiveness of automated recognition and tracking algorithms. Objects behind the distorting layers become nearly impossible to recognize using methods designed to operate in non-distorted environments. To address the challenges posed by Atmospheric Turbulence in video processing, current learning-based approaches typically adopt a range of strategies. Some methods focus on enhancing the visual quality

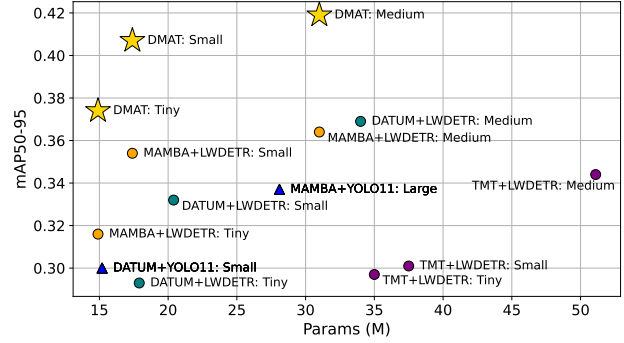


Figure 1. Object detection results for all object sizes and classes of our proposed method (DMAT) compared to individual AT-mitigation and object detection methods.

of videos before applying object detection to the restored outputs [15, 25]. Others retrain existing object detectors on synthetic datasets of atmospheric turbulence [37]. Another strategy includes integrating motion maps, which represent displacements caused by spatial distortions, into the network inputs of the object detectors [29]. Alternatively, some modify the detector's network architectures to better handle turbulence-induced distortions [16, 20]. In contrast to these methods, we introduce a novel approach that aggregates information in order to enhance feature quality, effectively enabling simultaneous video restoration and object detection within a cohesive, hybrid framework.

Existing methods have achieved considerable success in mitigating atmospheric turbulence; however, they often fail to ensure that restored or enhanced imagery is optimally configured for automatic object detection. A key challenge is that techniques effective in reducing wavy or ripple effects may inadvertently remove crucial features necessary for object identification within video sequences. To address this, this paper proposes a solution called DMAT (Detection and Mitigation of Atmospheric Turbulence), that not only enhances visual quality but also improves object detection accuracy, as demonstrated in Fig. 1, where our combined architecture outperforms individual AT-mitigation and object detection methods. Our approach aims to strike a bal-

ance between video enhancement and practical applicability in surveillance systems, ensuring improvement in both domains.

In this paper, we introduce a novel method that leverages 3D deformable convolutions and Structured State Space sequence (S4) models, known as Mamba. This approach addresses spatial displacement across the temporal domain, mitigates distortions such as blur, and enhances contrast. It is specifically designed to restore images affected by atmospheric turbulence and subsequently feed them into an object detector, which outputs object locations and classifications. Our joint framework is trained end-to-end with carefully designed loss functions, enabling the high-level features from the object detector and the low-level features from the turbulence mitigator to mutually enhance each other, resulting in significant improvements in both visual quality and object detection accuracy.

The main contributions of this paper are summarized as follows.

- A first end-to-end architecture for joint AT mitigation and object detection. We refer to this combined architecture as DMAT (Detection and Mitigation of Atmospheric Turbulence).
- A new optimized set of synthetic turbulent videos based on subsets of the COCO dataset.
- Benchmarking the end-to-end system (DMAT) against a range of individually applied mitigation and detection systems.

2. Related work

2.1. Atmospheric turbulence removal

Atmospheric turbulence is a limiting factor in the imaging of distant objects, degrading visual quality and impairing the performance of automated object recognition and tracking systems. Image sequences captured in turbulent environments often exhibit blurring and rippling effects, accompanied by fluctuations in light intensity across the scene. This phenomenon is particularly pronounced in environments characterized by intense heat, such as deserts, heated road surfaces, and areas surrounding man-made heat sources. Moreover, atmospheric turbulence exacerbates challenges in long-distance imaging applications, such as surveillance, especially when compounded by additional factors such as fog or haze, which further degrade image clarity and quality. Other environmental parameters, including wind speed, altitude, and humidity, also contribute to the severity of these distortions.

Given the spatio-temporal variability of atmospheric turbulence, restoring a scene distorted by atmospheric turbulence is a challenging problem. Traditional methods have involved frame selection, image registration, image fusion, phase alignment and image deblurring [2, 40, 45]. Re-

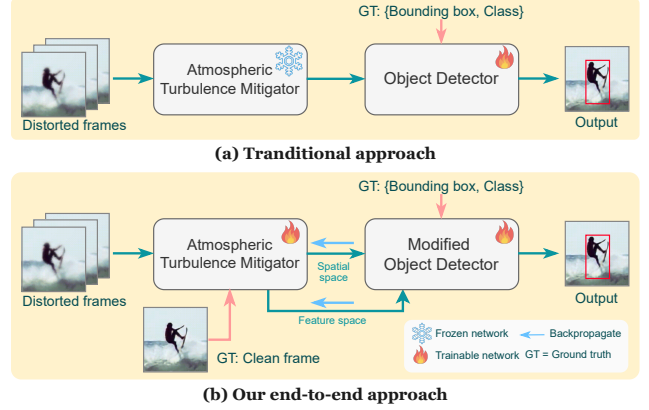


Figure 2. Diagrams of (a) transitional approach and (b) our proposed approach for joint restoration and object detection under atmospheric turbulence.

moving the turbulence distortion from a video containing moving objects is very challenging, as generally multiple frames are used and they are needed to be aligned. Temporal filtering with local weights determined from optical flow is employed to address this by Anantrasirichai et al. [1]. However, artefacts in the transition areas between foreground and background regions can remain. Removing atmospheric turbulence based on single image processing is proposed using ML by Gao et al. [9]. Deep learning techniques to solve this problem are still in their early stages. However, one method reported employs a CNN to support deblurring [28] and another employs multiple frames using a GAN architecture [7]. This however appears only to work well for static scenes.

Similar to de-hazing, physics-inspired models have been widely developed to remove turbulence distortion [17, 18], while complex-valued CNNs have been proposed to exploit phase information [3]. There was also an attempt to use implicit neural representation (INR) to solve this problem, offering tile and blur correction [18]. However, diffusion models outperform on a single image [27], and transformer-based methods remain state-of-the-art for restoring videos [44, 47]. A recent review can be found in [14].

2.2. Object Detection

Object detection involves both classification and localization, determining the presence of objects and their precise positions within visual inputs. The complexity of object detection arises from challenges such as varying object scales, occlusions, and diverse backgrounds. State-of-the-art object detection methods are most often based on three core components: i) *Backbone Network*: A deep CNN, often pre-trained on large datasets, serves as the feature extractor. Architectures such as ResNet [13] and MobileNetV4 [30] are commonly employed; ii) *Neck*: Intermediate layers within

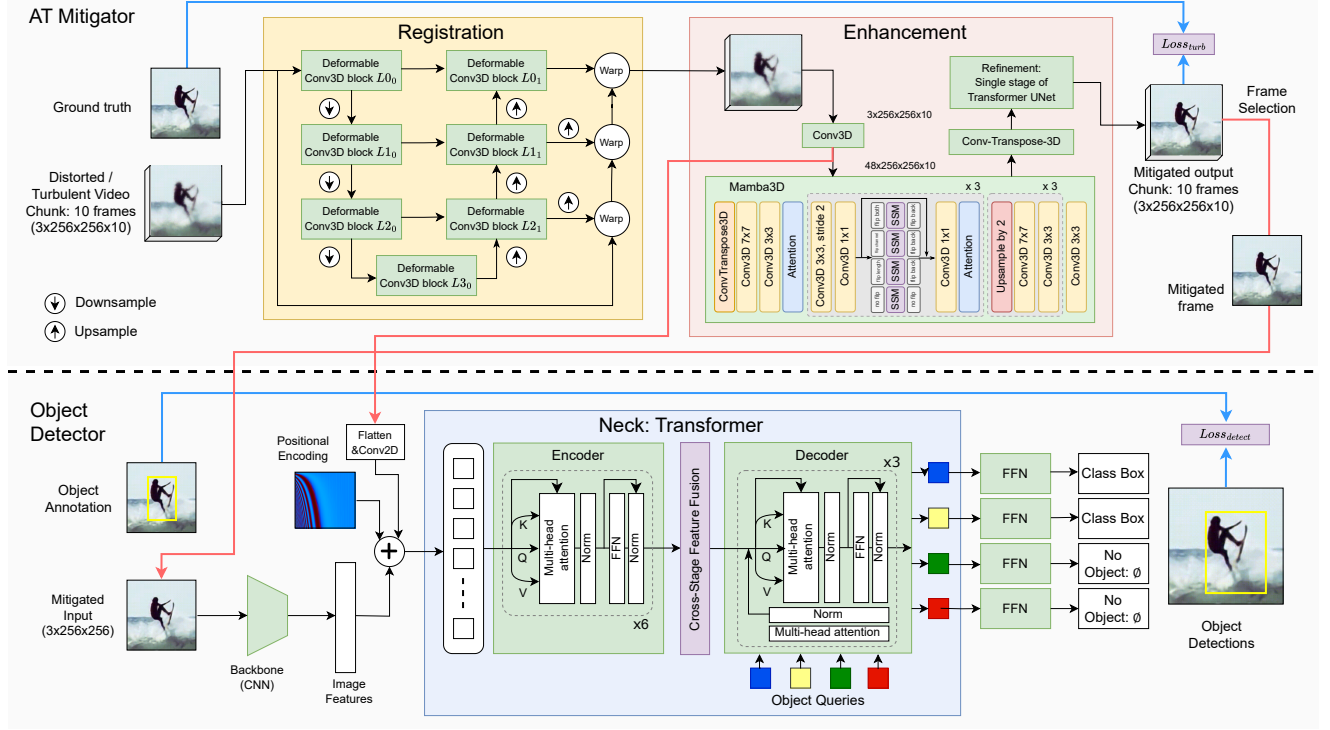


Figure 3. Architecture of the proposed DMAT framework for atmospheric distortion mitigation and object detection.

the neck component process features from the backbone to enhance semantic information across different scales. Examples include Feature Pyramid Networks (FPN) [21] and Path Aggregation Networks (PANet) [23]; iii) *Head/s*: The final layers predict bounding boxes and class probabilities. Depending on the model, this can involve anchor-based or anchor-free mechanisms. These models are broadly categorized into two-stage and one-stage detectors.

For two-stage detectors, conventional detectors, exemplified by the Region-based Convolutional Neural Network (R-CNN) family, first generate region proposals and subsequently classify each proposal. The original R-CNN [11] employed a selective search to extract region proposals, followed by feature extraction using a Convolutional Neural Network (CNN) and classification. Enhancements to R-CNN, such as Fast R-CNN [10] and Faster R-CNN [34] improve efficiency by integrating proposal generation and classification into a unified framework.

For one-stage detectors, the detectors process in a single forward pass, making them significantly faster than two-stage detectors. They predict bounding boxes and class probabilities directly, without requiring Region Proposal Networks (RPN). These models are widely used in real-time applications such as autonomous vehicles and surveillance systems. YOLO (You Only Look Once) [31] is one of the most popular detectors that formulate detection as a regres-

sion problem. The model divides an image into a grid and predicts bounding boxes and class probabilities in a single forward pass. Variants of YOLO include YOLOv2 [32] introducing anchor boxes, YOLOv3 [33] adding multi-scale detection, YOLOv4 [4] introducing data augmentation and CIoU loss, and recently YOLOv11 [19], incorporating advanced techniques to further boost performance. YOLO is widely used in real-time applications due to its speed and efficiency, though it can struggle with small objects and occlusions.

Transformer-based approaches have also gained attention. The DETR (DEtection TRansformer) [6] eliminates the need for anchor boxes and non-maximum suppression by using bipartite matching. This architecture consists of a transformer encoder-decoder that processes image features extracted from a convolutional backbone. Later, Deformable DETR [46] improves upon the original model by incorporating multi-scale deformable attention, making it more efficient and better suited for detecting small objects and DINO [41]; enhancing convergence speed and accuracy by introducing improved training strategies.

3. Methodology

Traditionally, models for AT mitigation and object detection are optimized separately. The AT mitigator is typically trained on synthetic datasets due to the absence of ground

truth information, where clean videos are pixel-wise registered to the distorted ones. Post-training, the AT mitigator is deployed to generate restored frames that are then utilized to fine-tune the object detector, as illustrated in Fig. 2 (a). In contrast, we propose a joint optimization strategy, as shown in Fig. 2 (b), where high-level features from the object detector guide the AT mitigator in discerning low-level features with semantic significance. Simultaneously, the object detector benefits from receiving more precise features from the AT mitigator, leading to improved overall performance. This synergistic approach promises to significantly advance the efficacy of both video restoration and object detection in atmospherically challenging conditions.

3.1. Overview

The architecture of our proposed framework is depicted in Fig. 3. This takes in a sequence of AT-distorted video frames and outputs restored video frames, along with the locations and categories of objects identified within these frames. Our framework consists of two primary modules: (1) *AT Mitigator*: This module processes the distorted frames to mitigate the atmospheric effects using a 3D Mamba structure; (2) *Modified Object Detector*: Leveraging a transformer-based model, this module is designed for lightweight and robust object detection. Note that the implementation can be adapted to other detection models as needed. The integration of these two modules occurs through (1) direct concatenation and (2) by feeding features extracted after the AT mitigator into the detection head, reducing redundancy in the feature extraction process of the traditional object detector.

3.2. AT Mitigation

Our AT mitigation module offers a robust solution to the problem of AT distortion, particularly the wavy effect, where there is a time-varying shift of features. Similar to other video processing frameworks, we input a group of frames and treat them as 3D data blocks. Since consecutive frames are highly correlated temporally but spatially shifted due to turbulence, the first step of our method (Registration module) is to register neighboring frames to the current frame. This process is necessary and has been employed with slight variations in both traditional model-based methods [2, 45] and deep-learning-based methods [44, 47].

Registration module. We incorporate a UNet-like architecture with deformable 3D convolutions implemented at all scales in both the encoder and decoder, denoted ‘Deformable Conv3D block’ in Fig. 3. This configuration is specifically designed to effectively estimate pixel shifts at different scales across frames. The deformable 3D convolutions enable pixel mappings associated with the current convolution kernel to extend beyond the conventional grid search area, accommodating spatio-temporal varia-

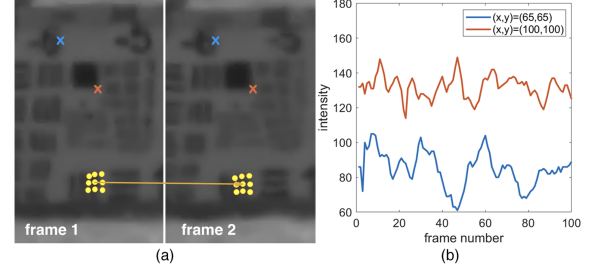


Figure 4. AT distortion. (a) Frame 1 and 2. (b) Temporal variation showing intensity changes of two pixels over time. Yellow dots visualize the benefit of deformable convolutions.

tions. This adaptability ensures that identical objects in different frames, even when subjected to varying turbulent distortions, can be aligned to exhibit consistent features as illustrated in Fig. 4.

The registration module has a depth scale of 4 ($L0-L3$) with kernel sizes of $3 \times 7 \times 7$, $3 \times 7 \times 7$, $3 \times 5 \times 5$, and $3 \times 3 \times 3$. Larger kernels are used in the initial layers to provide a wider field of view. The feature spaces expand to 32, 128, 128, and 256, with 3D batch normalization and max pooling for encoder downsamplers, while trilinear interpolation is used for decoder upsamplers. The output of each scale is a motion field which is then used for frame registration. The registered frames are then fed to the enhancement module.

Enhancement module. The first step consists in feature extraction using 3D convolutions with a kernel size of $3 \times 7 \times 7$. The features are then processed in the 3D Mamba-based UNet-like network and simultaneously fed to the object detector, as shown by the red line in Fig. 3. We also employ a UNet-like architecture but incorporate 3D Mamba at the encoder, which our studies have shown to outperform the 3D Swin Transformer [24], in agreement with the findings reported in [14]. The Mamba framework is based on the Structured State Space sequence (S4) model. It dynamically adjusts State Space Model (SSM) parameters in response to varying inputs, effectively addressing the common memory and gradient challenges associated with traditional SSM implementations.

Our 3D Mamba-based UNet-like network is based on nn-Mamba, proposed in [12], in which the encoder is structured with three layers of residual Mamba blocks (Res-Mamba), while the decoder utilizes a series of three double convolution blocks. To improve efficiency, we integrated an initial 3D convolution before the Mamba module that expands the temporal dimension in order for the 3D Mamba-based UNet-like structure to effectively treat the spatio-temporal tensor as a 3D tensor.

The Res-Mamba block integrates double convolution layers, skip connections, and a Mamba-in-convolution block that incorporates SSM functionalities between con-

volution, as detailed in the following equation:

$$F_o = \text{Conv}_1(\text{SSM}(\text{Conv}_1(F_i))) + \text{Conv}_1(F_i), \quad (1)$$

where F_i and F_o represent the input and output feature maps of the Res-Mamba block, respectively, within a 3D convolution context. $\text{Conv}_1(\cdot)$ is executed with a kernel size of $1 \times 1 \times 1$, followed by batch normalization and ReLU activation. $\text{SSM}(\cdot)$ is a selective SSM layer, trained using four augmented feature inputs, each flipped and rotated differently [12]. This sophisticated configuration culminates in the application of two Transformer blocks for optimal channel adjustment and refinement of the final output before passing it to the object detector.

3.3. Object Detection

The object detector in our framework is based on a Transformer architecture. Features from the mitigated frame, which is the output of the enhancement module, are extracted using a ResNet50 backbone. These features, along with those from the output of the registration process, are flattened and supplemented with positional encoding before being fed into a transformer encoder. The integration of the registration output features ensures that semantic insights from the object detector inform both modules in the AT mitigator, enhancing learning across the entire framework.

Similar to many other transformer-based methods for computer vision tasks, our encoder concatenates six transformer blocks. Each block comprises a multi-head self-attention module, batch normalization, and a feed-forward network (FFN). Inspired by LW-DETR [8] and YOLOv7 [38], we employ cross-stage feature fusion to improve gradient flow between the encoder and decoder. Our decoder consists of three transformer decoder blocks, each featuring a self-attention module, a cross-attention module, batch normalization, and an FFN. Finally, the FFNs are used to output the object category, box size and box location.

We provide three object detection model sizes. The increased size is reflected in an increase in the number of attention heads, number of transformer layers, embedding dimensions and backbone depth.

3.4. Loss function

The loss function is computed from two sources: the AT mitigator and the object detector, defined as $\text{Loss}_{\text{turb}}$ and $\text{Loss}_{\text{detect}}$, respectively. For $\text{Loss}_{\text{turb}}$, we employ the Charbonnier loss function, which merges the benefits of ℓ_1 and ℓ_2 losses, effectively managing outliers in pixel-wise error due to spatial variation from atmospheric turbulence. It is defined as:

$$L_{\text{Char}}(x, y) = \sqrt{(x - y)^2 + \epsilon^2}, \quad (2)$$

where x and y are the predicted and true values, and ϵ is a small constant (e.g., $1e - 3$) to ensure numerical stability.

The Charbonnier loss provides a smooth gradient even for small errors, making it ideally suited for addressing subtle discrepancies in turbulence-impacted images.

For $\text{Loss}_{\text{detect}}$, three loss functions are combined: L_{boxes} , L_{IoU} , and L_{labels} . L_{boxes} is an ℓ_1 regression loss for box size and location, while L_{IoU} represents the generalized IoU loss [35]. For L_{labels} , we use the Binary Cross-Entropy (BCE) loss to compute the probability p_{ce} of class accuracy, using the Intersection over Union (IoU) score. L_{labels} is defined as shown in Eq. 3 [5],

$$L_{\text{labels}} = -\frac{1}{N_{\text{pos}} + N_{\text{neg}}} \left[\sum_{N_{\text{pos}}} t \log p_{\text{ce}} + (1 - t) \log(1 - p_{\text{ce}}) + \sum_{N_{\text{neg}}} p_{\text{ce}}^\gamma \log(1 - p_{\text{ce}}) \right], \quad t = p_{\text{ce}}^\alpha \text{IoU}^{(1-\alpha)} \quad (3)$$

where N_{pos} and N_{neg} are the numbers of positive and negative boxes, γ controls the weight and is set to 2, and t is a smooth transition parameter between a positive target and a negative target, which is set to an exponential decay with $\alpha = 0.25$.

3.5. Alternating training strategy

Several strategies were considered for incorporating these losses within the training process. One approach involved combining the losses into a single, weighted objective function, enabling joint backpropagation through both networks during each training iteration. However, evaluation tests demonstrated that an alternating optimization scheme yielded improved performance. Specifically, dedicating separate training iterations to optimizing the quality of the mitigated output produced more favorable results. In contrast, the use of a combined weighted loss consistently led to degraded mitigation performance, regardless of the chosen weighting parameters. Therefore, we adopt an alternating training strategy for joint optimization of the mitigation and detection modules. Specifically, during odd-numbered iterations, the entire mitigation model is trained while the object detector remains frozen. In even-numbered iterations, we freeze the mitigation model (except for its last 10 layers) and train both the object detector and these unfrozen layers of the mitigator.

4. Datasets and implementation

4.1. Synthetic dataset

We employ the COCO2017 dataset [22], extracting various processed subsets to train and evaluate the combined DMAT system. The COCO2017 dataset includes over 330,000 images, where over 200,000 images are labeled with object instances, 80 object categories are annotated with bounding boxes and segmentation masks, and there are over 5 million object instance annotations.

4.1.1. Training, Validation, and Test Sets:

COCO is split into three sets: i) *Training Set*: Contains 118,000 images and over 2.5 million object instances; ii) *Validation Set*: Consists of 5,000 images with 80 object categories; iii) *Test Set*: Composed of 41,000 images. The test set annotations are not publicly available but are used for evaluation. Due to the unavailability of COCO test set annotations we have used the validation dataset for testing in our experiments.

4.1.2. Processed Subsets of the COCO Dataset:

In order to evaluate the developed system for different use-cases, we have subsampled the number of categories into three distinct application subsets:

- **All**: All of the 80 categories of the original COCO dataset.
- **Top10**: The top 10 most frequently found categories within the COCO training dataset: Person, Car, Chair, Book, Bottle, Cup, Dining Table, Bowl, Skis, and Handbag.
- **CarPerson**: Just the Car and Person classes (intended for surveillance applications).

4.1.3. Reduced Image Resolution:

The combined turbulence and object detection models use significant amounts of GPU memory due to: (i) the processing of spatio-temporal chunks across several hierarchical levels, and (ii) the large amount of memory required for processing images within the visual transformer structure. We have therefore reduced the resolution of all COCO input images in order to fit the processing of the data into the available GPU memory.

To ensure that object bounding boxes are not truncated upon image cropping, we filter all of the training and validation subsets so that only cropped 256×256 regions that wholly contain all objects in the image are included. This significantly reduces the number of images in the training and validation COCO subsets. However, due to the computational complexity of processing videos during training, the resulting number of images remains large but manageable for training. Furthermore, cropping subsets of the dataset has the advantage that all of the images (and therefore videos) being of a consistent resolution (256×256).

4.1.4. Synthetic AT Distortion:

We utilized the Phase-to-Space (P2S) Transform [26], a turbulence generation system developed at Purdue University, to efficiently simulate imaging through atmospheric turbulence. We evaluated this method as the best performing synthetic turbulence generation method currently available. The P2S method is based on three key steps: i) *Reformulating Spatially Varying Convolutions*: Converting these convolutions into a set of invariant convolutions with learned basis functions. ii) *Learning Basis Functions*: Using known

Table 1. Number of videos in each sub-sampled COCO dataset.

	All	Top10	CarPerson
Training	4594	5000	5000
Validation	503	668	831

turbulence statistical models to derive optimized basis functions. iii) *Implementing the P2S Transform*: Transforming phase representations into spatial turbulence effects. The output of the P2S transform is labeled as AT (atmospheric transform) in the results.

4.1.5. Final Training and Validation Video Datasets:

After extracting subsets from the COCO dataset, reducing the resolution to 256×256 , and generating 50-frame turbulent videos of the same spatial dimensions, we created training and validation video datasets as shown in Table 1 (a similar set of ground truth videos, labeled as noAT in the graphs below, were created that contained 50 identical frames).

4.2. Evaluation metrics

4.2.1. Object detection task:

Following the COCO dataset recommended evaluation, we use the standard metric based on the Average Precision (AP) across multiple intersection-over-union (IoU) thresholds. The metric measures the precision and recall of a detection model. The AP is calculated as the area under the Precision-Recall curve. It aggregates the precision-recall values for different IoU thresholds (typically from 0.50 to 0.95 with a step size of 0.05, referred to as AP[0.50-0.95]). This results in a metric that evaluates the model’s performance at various levels of localization precision. We report a Mean Average Precision (mAP). This is a summary metric that combines average precision (AP) across multiple object categories.

4.2.2. AT mitigation task:

We evaluate the performance of AT mitigation using the synthetic dataset; therefore, objective metrics can be used. These include Peak Signal-to-Noise Ratio (PSNR), Structural Similarity Index Measure (SSIM) [39], and perceptual similarity metrics like LPIPS [42].

4.3. Experiment settings

We compare our proposed method, DMAT, with three state-of-the-art AT mitigation methods, TMT [44], DATUM [43], and MAMBA [12], and three object detectors, YOLO11 [36], DETR [6], and LWDETR [8] with various model sizes.

The DATUM and TMT AT-mitigation models were used with pre trained weights. The Mamba model was pre-trained using the (256×256) training COCO dataset de-

scribed above. Optimization was performed using the Adam optimizer with an initial learning rate set to 0.0001. The model was trained for a total of 100 epochs without the use of early stopping criteria. These conditions were also used for training the combined system DMAT. A sliding window approach was employed for video processing, wherein a set of temporally adjacent frames centred on the current frame was used as input to predict the target frame. This strategy was uniformly applied during both the training and inference stages. In accordance with the findings reported in [3], a window of ten neighboring frames (four forward frames and five backward frames) was adopted, as it achieved good results but also was able to effectively represent temporal correlations.

Object detectors are fine-tuned by taking the pretrained weights of a network and updating them through training on new data, where the inherent AT distortions have been mitigated by the approaches mentioned above. Upper model layers are often frozen to preserve the representations of low-level visual content. In our training system, however, we update all layers within the object detector (as discussed below).

The implementation was carried out in Python, utilizing the PyTorch framework with CUDA acceleration to ensure computational efficiency. All experiments were conducted on a high-performance computing environment featuring NVIDIA 4090 and A100 GPUs.

5. Results and discussion

5.1. Performance of object detection

The results presented in Table 2 demonstrate that our proposed DMAT framework outperforms existing methods in object detection under AT conditions. Among two-stage approaches employing the same object detector, MAMBA achieves higher performance than TMT and DATUM. However, compared to our proposed DMAT, its performance can be up to 25% lower when using models of similar size. This highlights the effectiveness of our joint framework, where the AT mitigator generates restored frames with semantically enriched features that are more conducive to accurate object detection.

Figures 5a, 5b and 5c present the object detection performance of our DMAT in comparison with a variety of independently and sequentially applied baseline models. The graphs include detection results for the non mitigated ground truth (noAT) and turbulent (AT) inputs, serving as benchmarks for upper-bound and lower-bound performances, respectively. The results from the individual models reveal several trends: (i) detection performance generally improves with increasing model size; (ii) the Mamba-based AT mitigation model yields superior performance relative to DATUM and TMT in all cases.

The right hand side of figures 5a, 5b and 5c display the same set of methods evaluated specifically on small objects (defined as those smaller than 32×32 pixels), using mAP[0.50-0.95] as the performance metric. These graphs further illustrate that: (i) for all methods, mAP[0.50-0.95] degrades significantly when limited to small objects, which is expected due to the increased blurring effect of turbulence on smaller targets, even when AT-mitigation is applied; and (ii) the DMAT models maintain a performance advantage over individual methods, consistent with the trends observed across all object sizes.

Fig. 6 shows some example detections. All the shown methods apart from DMAT use the medium sized LW-DETR method (28.2 Million parameters) whereas the DMAT method uses the Medium sized architecture. This shows that object detection is obviously difficult for the distorted input (AT), improves with mitigation, and confirms that DMAT achieves superior performance.

5.2. Performance of AT mitigation

Table 3 shows objective comparison results of each AT mitigation method (compared to the ground truth no-AT sequences). This table shows that the DMAT method gives the best performance in terms of distortion measured by PSNR and SSIM. This superior performance may be attributed to its additional training stages that explicitly incorporate a distortion loss. Alternatively, or in conjunction, the enhanced results could stem from the joint optimization of the object detection loss, which likely contributes to improved structural fidelity in the reconstructed objects.

Fig. 7 presents a subjective comparison of the results from DMAT compared with TMT, DATUM and MAMBA methods. Subjectively, DATUM preserves textures the best, but turbulence effects remain at the object edges. TMT produces sharper edges but at the expense of texture loss. The MAMBA method strikes a balance between the two, offering a compromise on texture preservation and edge definition. When incorporating the object detector, our DMAT method enhances sharpness around foreground objects but sacrifices texture details in the background compared to the MAMBA method.

6. Conclusion

In this paper, we introduce the first end-to-end framework that jointly addresses AT mitigation and object detection. By tightly coupling a 3D Mamba-based turbulence mitigation module with a transformer-based object detector, the proposed architecture enables mutual enhancement between low-level restoration features and high-level semantic representations. This integration not only preserves crucial object-level details often lost during restoration but also significantly improves detection accuracy under severe atmospheric distortions. Extensive experiments on synthetically

Table 2. Object detection performance in terms of mAP[0.50-0.95] for AT mitigation methods and detectors across COCO subsets and object sizes. Results in gray indicate ‘no AT’ (i.e., undistorted inputs from COCO images), served as upper-bound performance. The top three results in each column are highlighted in green, orange, and yellow, respectively. ‘AT’ refers to non-mitigated, distorted inputs affected by atmospheric turbulence (simulated using P2S). Parameters column shows number of parameters in the object detector and (where applicable) the additional number of parameters in the AT-mitigator

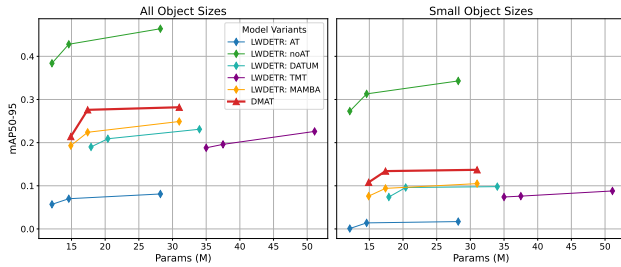
AT Mitigation	Detector	Params (M)	AllCls-AllSz	AllCls-Small	Top10-AllSz	Top10-Small	CarPerson-AllSz	CarPerson-Small
no AT	YOLO11n	2.6	0.419	0.089	0.279	0.080	0.437	0.313
	YOLO11s	9.4	0.509	0.099	0.364	0.095	0.505	0.370
	YOLO11m	20.1	0.547	0.122	0.410	0.107	0.547	0.417
	YOLO11l	25.3	0.548	0.129	0.430	0.110	0.569	0.430
	YOLO11x	56.9	0.576	0.133	0.450	0.114	0.590	0.451
	DETR-Med	41.3	0.483	0.307	0.312	0.204	0.448	0.309
	DETR-Large	60.0	0.525	0.363	0.346	0.234	0.468	0.468
	LWDETR-Tiny	12.1	0.523	0.410	0.384	0.273	0.505	0.375
	LWDETR-Small	14.6	0.561	0.431	0.428	0.313	0.534	0.400
	LWDETR-Med	28.2	0.628	0.480	0.464	0.343	0.566	0.427
AT	YOLO11n	2.6	0.050	0.010	0.020	0.004	0.062	0.014
	YOLO11s	9.4	0.090	0.014	0.040	0.004	0.099	0.020
	YOLO11m	20.1	0.093	0.012	0.040	0.005	0.104	0.022
	YOLO11l	25.3	0.101	0.010	0.040	0.005	0.114	0.022
	YOLO11x	56.9	0.124	0.029	0.060	0.009	0.148	0.034
	DETR-Med	41.3	0.092	0.035	0.031	0.003	0.092	0.021
	DETR-Large	60.0	0.066	0.026	0.035	0.008	0.104	0.025
	LWDETR-Tiny	12.1	0.158	0.068	0.057	0.000	0.136	0.039
	LWDETR-Small	14.6	0.149	0.073	0.070	0.014	0.147	0.049
	LWDETR-Med	28.2	0.192	0.061	0.081	0.017	0.164	0.049
DATUM	YOLO11n	5.8+2.6	0.128	0.034	0.110	0.026	0.217	0.097
	YOLO11s	5.8+9.4	0.300	0.054	0.134	0.038	0.259	0.117
	YOLO11m	5.8+20.1	0.307	0.057	0.151	0.033	0.276	0.130
	YOLO11l	5.8+25.3	0.301	0.065	0.151	0.035	0.289	0.131
	YOLO11x	5.8+56.9	0.317	0.060	0.166	0.032	0.291	0.132
	DETR-Med	5.8+41.3	0.218	0.076	0.108	0.034	0.195	0.074
	DETR-Large	5.8+60.0	0.243	0.100	0.120	0.051	0.216	0.087
	LWDETR-Tiny	5.8+12.1	0.293	0.158	0.190	0.074	0.265	0.120
	LWDETR-Small	5.8+14.6	0.332	0.167	0.209	0.096	0.289	0.134
	LWDETR-Med	5.8+28.2	0.369	0.200	0.231	0.098	0.306	0.140
TMT	YOLO11n	22.9+2.6	0.229	0.029	0.107	0.021	0.203	0.082
	YOLO11s	22.9+9.4	0.294	0.028	0.149	0.024	0.241	0.094
	YOLO11m	22.9+20.1	0.276	0.042	0.154	0.028	0.242	0.092
	YOLO11l	22.9+25.3	0.301	0.054	0.161	0.028	0.263	0.111
	YOLO11x	22.9+56.9	0.307	0.038	0.168	0.026	0.256	0.092
	DETR-Med	22.9+41.3	0.204	0.062	0.101	0.029	0.162	0.045
	DETR-Large	22.9+60.0	0.224	0.087	0.129	0.040	0.178	0.052
	LWDETR-Tiny	22.9+12.1	0.297	0.134	0.188	0.074	0.237	0.097
	LWDETR-Small	22.9+14.6	0.301	0.143	0.196	0.076	0.257	0.106
	LWDETR-Med	22.9+28.2	0.344	0.165	0.226	0.088	0.271	0.119
MAMBA	YOLO11n	2.8+2.6	0.249	0.024	0.120	0.026	0.228	0.098
	YOLO11s	2.8+9.4	0.310	0.038	0.176	0.028	0.267	0.117
	YOLO11m	2.8+20.1	0.312	0.046	0.177	0.030	0.285	0.130
	YOLO11l	2.8+25.3	0.337	0.055	0.179	0.031	0.294	0.135
	YOLO11x	2.8+56.9	0.350	0.037	0.191	0.031	0.292	0.128
	DETR-Med	2.8+41.3	0.227	0.073	0.113	0.031	0.200	0.067
	DETR-Large	2.8+60.0	0.275	0.097	0.135	0.041	0.217	0.076
	LWDETR-Tiny	2.8+12.1	0.316	0.164	0.193	0.076	0.270	0.115
	LWDETR-Small	2.8+14.6	0.354	0.161	0.224	0.094	0.295	0.136
	LWDETR-Med	2.8+28.2	0.364	0.186	0.249	0.105	0.310	0.138
	DMAT-Tiny (ours)	2.8+12.1	0.374	0.188	0.214	0.108	0.348	0.178
	DMAT-Small (ours)	2.8+14.6	0.407	0.234	0.276	0.134	0.373	0.194
	DMAT-Med (ours)	2.8+28.2	0.419	0.234	0.282	0.137	0.385	0.199

generated turbulent datasets derived from the COCO benchmark demonstrated that our combined system outperforms both individually trained AT-mitigation and object detection pipelines. Notably, the unified architecture yielded up to a 15% improvement in mAP[0.50-0.95] across var-

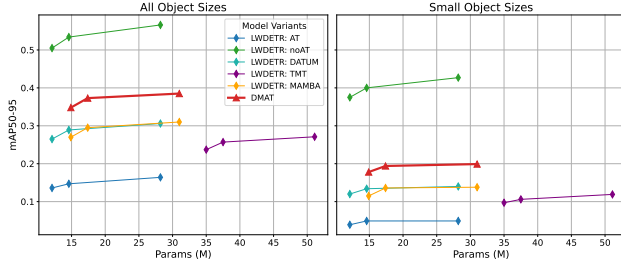
ious detector types and turbulence conditions, and maintained strong performance even on challenging subsets such as small object categories and surveillance-focused object classes. These results highlight the advantages of bidirectional feature flow in restoring spatial-temporal consistency

Table 3. Comparison of AT Mitigation methods using Mean PSNR, SSIM, and LPIPS metrics across three datasets: All, CarPerson, and Top10 categories. Best values are highlighted in green, second in orange, third in yellow.

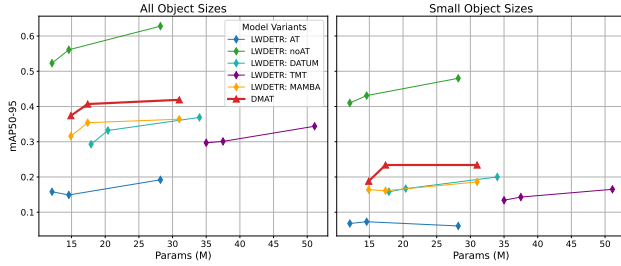
AT Mitigation	All			CarPerson			Top10		
	PSNR \uparrow	SSIM \uparrow	LPIPS \downarrow	PSNR \uparrow	SSIM \uparrow	LPIPS \downarrow	PSNR \uparrow	SSIM \uparrow	LPIPS \downarrow
AT (no mitigation)	20.946	0.512	0.546	20.210	0.488	0.564	20.668	0.513	0.550
DATUM	23.092	0.644	0.356	22.390	0.632	0.360	22.910	0.649	0.343
TMT	23.332	0.654	0.348	22.592	0.641	0.350	23.167	0.661	0.331
MAMBA	23.763	0.667	0.378	23.084	0.657	0.380	23.693	0.677	0.360
DMAT (ours)	23.841	0.671	0.373	23.220	0.663	0.376	23.861	0.683	0.357



(a) Top10 object classes



(b) CarPerson object classes



(c) All object classes

Figure 5. Object detection performance (mAP[0.50-0.95]) for various object class groupings across all (left) and small (right) object sizes. Number of parameters is the size of the object detector only (for AT and noAT) and the sum of parameters of the AT mitigation model and the object detector.

and enhancing detection robustness. The framework further shows that alternating loss function optimization—rather than weighted joint loss—achieves better convergence and

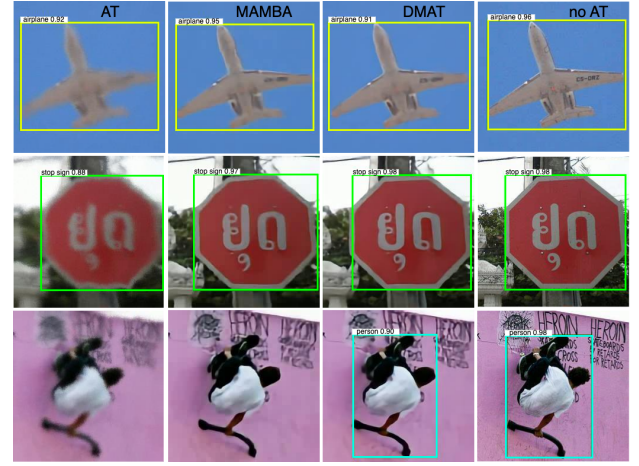


Figure 6. Comparison of AT-mitigation and Object Detection Methods. All methods apart from DMAT use the medium sized LW-DETR method (28.2 Million parameters) whereas the DMAT method uses the Medium sized architecture.

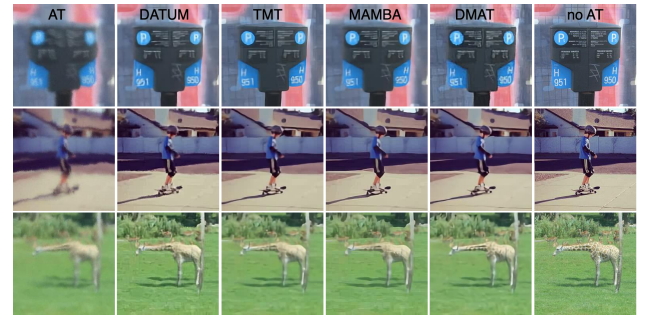


Figure 7. Comparison of AT-mitigation methods

output quality, mitigating the issue of visual degradation commonly observed when attempting to balance restoration and detection objectives. Although the combined architecture proposed gives superior performance compared to the non combined models and methods it does have a larger memory requirement due to the models needing to be loaded into memory together during training.

References

- [1] N. Anantrasirichai, A. Achim, and D. Bull. Atmospheric turbulence mitigation for sequences with moving objects using recursive image fusion. In *2018 25th IEEE International Conference on Image Processing (ICIP)*, pages 2895–2899, 2018.
- [2] N. Anantrasirichai, A. Achim, N.G. Kingsbury, and D.R. Bull. Atmospheric turbulence mitigation using complex wavelet-based fusion. *Image Processing, IEEE Transactions on*, 22(6):2398–2408, 2013.
- [3] Nantheera Anantrasirichai. Atmospheric turbulence removal with complex-valued convolutional neural network. *Pattern Recognition Letters*, 171:69–75, 2023.
- [4] Alexey Bochkovskiy, Chien-Yao Wang, and Hong-Yuan Mark Liao. YOLOv4: Optimal speed and accuracy of object detection. *arXiv preprint arXiv:2004.10934*, 2020.
- [5] Zhi Cai, Songtao Liu, Guodong Wang, Zeming Li, Zheng Ge, Xiangyu Zhang, and Di Huang. Align-DETR: Enhancing end-to-end object detection with aligned loss. In *35th British Machine Vision Conference 2024, BMVC 2024, Glasgow, UK, November 25–28, 2024*. BMVA, 2024.
- [6] Nicolas Carion, Francisco Massa, Gabriel Synnaeve, Nicolas Usunier, Alexander Kirillov, and Sergey Zagoruyko. End-to-end object detection with transformers. In *European Conference on Computer Vision (ECCV)*, pages 213–229, 2020.
- [7] Wai Ho Chak, Chun Pong Lau, and Lok Ming Lui. Subsampled turbulence removal network. In *arXiv:1807.04418v2*, 2018.
- [8] Qiang Chen, Xiangbo Su, Xinyu Zhang, Jian Wang, Jiahui Chen, Yunpeng Shen, Chuchu Han, Ziliang Chen, Weixiang Xu, Fanrong Li, et al. LW-DETR: A transformer replacement to yolo for real-time detection. *arXiv preprint arXiv:2406.03459*, 2024.
- [9] Jing Gao, N. Anantrasirichai, and David Bull. Atmospheric turbulence removal using convolutional neural network. In *arXiv:1912.11350*, 2019.
- [10] Ross Girshick. Fast r-cnn. In *Proceedings of the IEEE international conference on computer vision*, pages 1440–1448, 2015.
- [11] Ross Girshick, Jeff Donahue, Trevor Darrell, and Jitendra Malik. Rich feature hierarchies for accurate object detection and semantic segmentation. In *Proceedings of the IEEE conference on computer vision and pattern recognition*, pages 580–587, 2014.
- [12] Haifan Gong, Luoyao Kang, Yitao Wang, Xiang Wan, and Haofeng Li. nmmamba: 3d biomedical image segmentation, classification and landmark detection with state space model. *arXiv preprint arXiv:2402.03526*, 2024.
- [13] Kaiming He, Xiangyu Zhang, Shaoqing Ren, and Jian Sun. Deep residual learning for image recognition. In *Proceedings of the IEEE conference on computer vision and pattern recognition*, pages 770–778, 2016.
- [14] Paul Hill, Nantheera Anantrasirichai, Alin Achim, and David Bull. Deep learning techniques for atmospheric turbulence removal: a review. *Artificial Intelligence Review*, 58(4):101, 2025.
- [15] Paul Hill, Zhiming Liu, and Nantheera Anantrasirichai. MAMAT: 3d Mamba-based atmospheric turbulence removal and its object detection capability. *arXiv:2503.17700v1*, 2025.
- [16] Disen Hu and Nantheera Anantrasirichai. Object recognition in atmospheric turbulence scenes. In *31st European Signal Processing Conference (EUSIPCO)*, pages 561–565, 2023.
- [17] Ajay Jaiswal, Xingguang Zhang, Stanley H Chan, and Zhangyang Wang. Physics-driven turbulence image restoration with stochastic refinement. In *Proceedings of the IEEE/CVF International Conference on Computer Vision*, pages 12170–12181, 2023.
- [18] Weiyun Jiang, Vivek Boominathan, and Ashok Veeraraghavan. Nert: Implicit neural representations for unsupervised atmospheric turbulence mitigation. In *Proceedings of the IEEE/CVF Conference on Computer Vision and Pattern Recognition (CVPR) Workshops*, pages 4235–4242, June 2023.
- [19] Rahima Khanam and Muhammad Hussain. YOLOv11: An overview of the key architectural enhancements. *arXiv preprint arXiv:2410.17725*, 2024.
- [20] Chun Pong Lau, Hossein Souri, and Rama Chellappa. AT-FaceGAN: Single face image restoration and recognition from atmospheric turbulence. In *FG*, pages 32–39, 2020.
- [21] Tsung-Yi Lin, Piotr Dollár, Ross Girshick, Kaiming He, Bharath Hariharan, and Serge Belongie. Feature pyramid networks for object detection. In *Proceedings of the IEEE conference on computer vision and pattern recognition*, pages 2117–2125, 2017.
- [22] Tsung-Yi Lin, Michael Maire, Serge Belongie, James Hays, Pietro Perona, Deva Ramanan, Piotr Dollár, and C Lawrence Zitnick. Microsoft coco: Common objects in context. In *European Conference on Computer Vision (ECCV)*, pages 740–755. Springer, 2014.
- [23] Shu Liu, Lu Qi, Haifang Qin, Jianping Shi, and Jiaya Jia. Path aggregation network for instance segmentation. In *Proceedings of the IEEE conference on computer vision and pattern recognition*, pages 8759–8768, 2018.
- [24] Ze Liu, Yutong Lin, Yue Cao, Han Hu, Yixuan Wei, Zheng Zhang, Stephen Lin, and Baining Guo. Swin transformer: Hierarchical vision transformer using shifted windows. In *Proceedings of the IEEE/CVF international conference on computer vision*, pages 10012–10022, 2021.
- [25] Z. Mao, A. Jaiswal, Z. Wang, and S. H. Chan. Single frame atmospheric turbulence mitigation: A benchmark study and a new physics-inspired transformer model. In *Computer Vision – ECCV 2022*, 2022.
- [26] Zhiyuan Mao, Nicholas Chimitt, and Stanley H Chan. Accelerating atmospheric turbulence simulation via learned phase-to-space transform. In *Proceedings of the IEEE/CVF International Conference on Computer Vision*, pages 14759–14768, 2021.
- [27] Nithin Gopalakrishnan Nair, Kangfu Mei, and Vishal M Patel. At-ddpm: Restoring faces degraded by atmospheric turbulence using denoising diffusion probabilistic models. In *Proceedings of the IEEE/CVF Winter Conference on Applications of Computer Vision*, pages 3434–3443, 2023.

- [28] Robert Nieuwenhuizen and Klammer Schutte. Deep learning for software-based turbulence mitigation in long-range imaging. In *Artificial Intelligence and Machine Learning in Defense Applications*, volume 11169, pages 153 – 162. International Society for Optics and Photonics, SPIE, 2019.
- [29] D. Qin, R.K. Saha, W. Chung, S. Jayasuriya, J. Ye, and N. Li. Unsupervised moving object segmentation with atmospheric turbulence. In *Computer Vision – ECCV 2024*, volume 15064 of *Lecture Notes in Computer Science*. Springer, 2025.
- [30] Danfeng Qin, Chas Leichner, Manolis Delakis, Marco Fornoni, Shixin Luo, Fan Yang, Weijun Wang, Colby Banbury, Chengxi Ye, Berkin Akin, et al. Mobilenetv4: universal models for the mobile ecosystem. In *European Conference on Computer Vision*, pages 78–96. Springer, 2024.
- [31] Joseph Redmon, Santosh Divvala, Ross B. Girshick, and Ali Farhadi. You only look once: Unified, real-time object detection. In *IEEE Conference on Computer Vision and Pattern Recognition (CVPR)*, pages 779–788, 2016.
- [32] Joseph Redmon and Ali Farhadi. Yolo9000: Better, faster, stronger. In *IEEE Conference on Computer Vision and Pattern Recognition (CVPR)*, pages 7263–7271, 2017.
- [33] Joseph Redmon and Ali Farhadi. Yolo3: An incremental improvement. In *arXiv preprint arXiv:1804.02767*, 2018.
- [34] Shaoqing Ren, Kaiming He, Ross B. Girshick, and Jian Sun. Faster R-CNN: Towards real-time object detection with region proposal networks. *Advances in Neural Information Processing Systems (NeurIPS)*, 28:91–99, 2015.
- [35] Hamid Rezaatfighi, Nathan Tsoi, JunYoung Gwak, Amir Sadeghian, Ian Reid, and Silvio Savarese. Generalized intersection over union: A metric and a loss for bounding box regression. In *Proceedings of the IEEE/CVF Conference on Computer Vision and Pattern Recognition (CVPR)*, pages 658–666, 2019.
- [36] Author(s) Unknown. Yolo11: An overview of the key architectural enhancements, 2024. Accessed: 2025-04-11.
- [37] E. Uzun and E. Akagündüz. Augmenting atmospheric turbulence effects on thermal-adapted deep object detection models. *Scientific Reports*, 15:9900, 2025.
- [38] Chien-Yao Wang, Alexey Bochkovskiy, and Hong-Yuan Mark Liao. YOLOv7: Trainable bag-of-freebies sets new state-of-the-art for real-time object detectors. In *Computer Society Conference on Computer Vision and Pattern Recognition*, 2023.
- [39] Zhou Wang, Alan C Bovik, Hamid R Sheikh, and Eero P Simoncelli. Image quality assessment: from error visibility to structural similarity. *IEEE Transactions on Image Processing*, 13(4):600–612, 2004.
- [40] Y. Xie, W. Zhang, D. Tao, W. Hu, Y. Qu, and H. Wang. Removing turbulence effect via hybrid total variation and deformation-guided kernel regression. *IEEE Transactions on Image Processing*, 25(10):4943–4958, 2016.
- [41] Feng Zhang, Shilong Fang, Xuyang Li, Qian Zhang, Jian Sun, and Yike Wang. Dino: Detr with improved training and optimized prediction. *arXiv preprint arXiv:2203.03605*, 2022.
- [42] Richard Zhang, Phillip Isola, Alexei A Efros, Eli Shechtman, and Oliver Wang. Perceptual similarity metrics and the reliability of relative judgments. In *Proceedings of the IEEE/CVF Conference on Computer Vision and Pattern Recognition (CVPR)*, pages 10648–10657, 2021.
- [43] Xingguang Zhang, Nicholas Chimitt, Yiheng Chi, Zhiyuan Mao, and Stanley H Chan. Spatio-temporal turbulence mitigation: A translational perspective. *arXiv preprint arXiv:2401.04244*, 2024.
- [44] Xingguang Zhang, Zhiyuan Mao, Nicholas Chimitt, and Stanley H. Chan. Imaging through the atmosphere using turbulence mitigation transformer. *IEEE Transactions on Computational Imaging*, 10:115–128, 2024.
- [45] X. Zhu and P. Milanfar. Removing atmospheric turbulence via space-invariant deconvolution. *IEEE Transactions on Pattern Analysis and Machine Intelligence*, 35(1):157–170, 2013.
- [46] Xizhou Zhu, Weijie Su, Lewei Lu, Bin Li, Xiaogang Wang, and Jifeng Dai. Deformable detr: Deformable transformers for end-to-end object detection. In *International Conference on Learning Representations (ICLR)*, 2021.
- [47] Z. Zou and N. Anantrasirichai. Deturb: Atmospheric turbulence mitigation with deformable 3d convolutions and 3d swin transformers. In *Proceedings of the Asian Conference on Computer Vision (ACCV)*, 2024.